Optimizing flow properties of the different nanofluids inside a circular tube by using entropy generation minimization approach

Article *in* Journal of Thermal Analysis and Calorimetry · May 2018

DOI: 10.1007/s10973-018-7276-x

CITATIONS
3

READS
99

6 authors, including:

Behnam Mohseni-Gharyehsafa
Shahrood University of Technology
5 PUBLICATIONS **4** CITATIONS
SEE PROFILE

Vahab Okati
Chabahar Maritime University
6 PUBLICATIONS **8** CITATIONS
SEE PROFILE

Mohammad H. Ahmadi
Shahrood University of Technology
138 PUBLICATIONS **2,273** CITATIONS
SEE PROFILE

Journal of Thermal Analysis and Calorimetry
https://doi.org/10.1007/s10973-018-7276-x

Optimizing flow properties of the different nanofluids inside a circular tube by using entropy generation minimization approach

Behnam Mohseni-Gharyehsafa[1] · Amir Ebrahimi-Moghadam[2] · V. Okati[1,3] · Mahmood Farzaneh-Gord[1] · Mohammad Hossein Ahmadi[1] · Giulio Lorenzini[4]

Received: 27 February 2018 / Accepted: 4 April 2018

Abstract

The use of nanofluids as working fluid is one of the represented methods in efficiency enhancement of various systems. One of the most important subjects in nanofluid utilization is finding the optimal conditions. In this study, the efforts have been made to find optimal condition of forced convection nanofluid flow inside a circular tube. The flow is assumed turbulent, and optimization process is carried out for two metallic oxide nanoparticles (Al_2O_3, CuO) and one nonmetallic oxide nanoparticle (SiO_2), dispersed in a 60:40% ethylene glycol/water base fluid. The optimization process has been performed based on the second law of thermodynamic and entropy generation minimization approach. The process has been focused on finding the optimal values for volume fraction, Reynolds number, diameter of particles and average flow temperature. Results show that two metallic oxide nanofluids generate less entropy compared with nonmetallic oxide nanofluid. In addition, comparing these two metallic oxide nanofluids, the maximum amount of total entropy generation is 20% lower when CuO nanoparticles added to the base fluid instead of Al_2O_3.

Keywords Nanofluid · EGM method · Optimization

List of symbols

A	Cross-sectional area of the tube (m^2)
B	Duty parameter
Be	Bejan number
C_p	Specific heat (J kg^{-1} K^{-1})
D	Inside diameter of the tube (m)
d_p	Nanoparticle diameter (nm)
f	Friction factor
h	Heat transfer coefficient (W m^{-2} K^{-1})
k	Thermal conductivity (W m^{-1} K^{-1})
L	Length of the tube (m)
$\dot{m}$	Mass flow rate (kg s^{-1})
N_s	Entropy generation number
Nu	Nusselt number
Pr	Prandtl number
Q	Dimensionless heat flux
q	Heat transfer per unit tube length (W m^{-1})
q''	Heat flux (W m^{-2})
Re	Reynolds number
R^2	Coefficient of determination
$\dot{S}'_g$	Entropy generation rate per unit tube length (W m^{-1} K^{-1})
$S_{g,h}$	Entropy generation due to the heat transfer (W K^{-1})
$S_{g,f}$	Entropy generation due to the fluid friction (W K^{-1})
$S_{g,tot}$	Total entropy generation (W K^{-1})
St	Stanton number
T	Average flow temperature (K)
T_0	Reference temperature, 273 K

✉ Amir Ebrahimi-Moghadam
amir_ebrahimi_051@mshdiau.ac.ir

✉ Mohammad Hossein Ahmadi
mohammadhosein.ahmadi@gmail.com;
mhosein.ahmadi@shahroodut.ac.ir

[1] Faculty of Mechanical Engineering, Shahrood University of Technology, Shahrood, Iran

[2] Young Researchers and Elite Club, Mashhad Branch, Islamic Azad University, Mashhad, Iran

[3] Faculty of Marine Engineering, Chabahar Maritime University, Chabahar, Iran

[4] Dipartimento di Ingegneria e Architettura, Università degli Studi di Parma, Parco Area delle Scienze 181/A, 43124 Parma, Italy

Published online: 08 May 2018

Greek symbols

κ Boltzmann constant, 1.381×10^{-23} (J K^{-1})
μ Viscosity (Ns m^{-2})
ρ Density (kg m^{-3})
Φ Irreversibility distribution ratio
ϕ Particle volumetric concentration (%)

Subscripts

B Brownian motion
bf Base fluid
nf Nanofluid
opt Optimum
p Particle
s Static

Introduction

Nanofluids are a batch of fluids that are generally composed of two components: The first component is a typical fluid (such as water, mixture of water/ethylene glycol) and named base fluid, which the nanoparticles (the second component) are dispersed within it [1]. Nanofluids that are based on metal-oxide nanoparticles are recently used in many industrial applications for improving heat transfer performance [2, 3]. Nanofluids are widely used in various engineering applications such as microchannels [4–7], heat exchangers [8–11], solar collectors [12–15], heat pipes [16–18].

Although analyzing nanofluid flow using first law gives helpful information about efficiency of the heat transfer, it just provides little information about quality of available energy. Also based on first law analysis, it is not possible to optimize flow condition. These limitations could be overcome by taking advantage of the second law of thermodynamics.

The entropy generation minimization (EGM), as an engineering optimization method, is designed to make thermodynamics and heat transfer more efficient. The method optimizes real systems based on the second law of thermodynamics, by linking heat transfer and fluid flow [19].

The EGM method has been applied in various studies to design thermal systems and optimization of system components. On the other side, a lot of researchers have used the EGM method for calculating entropy generation in fluid flow and heat transfer for various applications. Farzaneh-Gord et al. [20] presented an investigation for optimizing tube-in-tube helical heat exchanger performance. They applied EGM for laminar and turbulent flows to find the optimum geometry and working conditions of this heat exchanger. An EGM analysis was developed by Gutierrez and Mendez [21] for the thermal cracking of methane gas to hydrogen. They numerically solved governing equations (the mass balance equation, energy balance equation and global entropy generation equation) and used genetic algorithms to obtain an optimal solution for the thermal design of the solar reactor.

There are many investigations utilizing the second law of thermodynamics to study the effects of nanofluid on heat transfer and the amount of entropy generation. But a limit researches have been carried out in order to minimize entropy generation rate and optimize nanofluid flow. Ellahi et al. [22] studied the shape effects of Nimonic 80a metal nanoparticles dispersed in HFE-7100 base fluid. They modeled the nanofluid flow over a wedge and examined the spherical and non-spherical shapes of the nanoparticles on the heat transfer and entropy generation. A computational fluid dynamics (CFD) method was developed by Siavashi and Jamali [23] to study the effect of the nanoparticles volume fraction, Reynolds number and the radius ratio of annuli on heat transfer and entropy generation rate. They applied this method to investigate a fully developed turbulent flow of TiO_2 nanofluid as a two-phase mixture. Shalchi-Tabrizi and Seyf [24] numerically simulated Al_2O_3 nanofluid flow in a tangential micro heat sink to investigate the effects of nanofluid utilization on entropy generation and convective heat transfer. The results of the study showed that total entropy generation decreases by increasing volume fraction, Reynolds number and decreasing size of particles. Bianco et al. [25] numerically analyzed the effect of using Al_2O_3-water nanofluid turbulent flow on heat transfer performance and the amount of the entropy generation, for circular tubes with constant wall temperature boundary condition. Singh et al. [26] prepared a theoretical investigation about entropy generation analysis of Al_2O_3/water nanofluid for various types of channels containing: microchannel (with 0.1 mm diameter), minichannel (with 1 mm diameter) and conventional channel (with 10 mm diameter). Torabi et al. [27] analyzed heat transfer and entropy generation of alumina–water nanofluid laminar flow. Their investigated model was a porous channel with some square pillars on channel's walls. The pillars were installed on the channel walls in staggered and in-line modes. A research was conducted by Mwesigye and Huan [28] to investigate the effects of pipe cross section and volume fraction of water-Al_2O_3 nanofluid on entropy generation. The governing equations were numerically solved for turbulent flow in a circular pipe.

In addition to the above-mentioned researches, there are more investigations focused on heat transfer and entropy generation calculation and optimization in nanofluid flows. However, little attention has been made to optimize the flow parameters by means of EGM. Considering the limited researches in this field, the main objective of current

investigation is to optimize nanofluids turbulent flow inside a circular tube. The top and bottom walls of the tube are exposed to different heat flues; this type of the boundary condition can be used as an approximate application in solar collectors. The optimization is carried out by utilizing the second law of thermodynamic and entropy generation minimization approach. For minimizing the rate of entropy generation, four parameters, namely nanofluid volume fraction (ϕ), nanoparticle diameter (d_p), average flow temperature (T) and Reynolds number, are optimized by applying quadratic optimization method. In addition, the optimization process is carried out for three common nanoparticles (namely Al_2O_3, CuO and SiO_2) dispersed in a 60:40% ethylene glycol/water base fluid.

Geometry and formulation

In this section, the detailed mathematical formulation of the nanofluid flow inside a circular tube based on the second law of thermodynamics is presented. Figure 1 shows the model under investigation that is made of a circular tube which receives different constant heat fluxes on walls. The length of the tube is 1.5 m and is made of copper (with 31 mm inside radius). Due to the different heat fluxes on tube walls, the problem can be considered as an application of the parabolic trough solar collectors [29].

By applying the first law and second law of thermodynamics, the rate of entropy generation (per unit length of the tube) for internal flows could be written as [30]:

$$\dot{S}'_g = \left(\dot{S}'_g\right)_{\text{thermal}} + \left(\dot{S}'_g\right)_{\text{frictional}} = \frac{q^2 D}{4T^2 \dot{m} C_{p,nf} St} + \frac{2\dot{m}^3 f_{nf}}{\rho_{nf}^2 \text{TDA}^2} \quad (1)$$

where $C_{p,nf}$ and ρ_{nf} are specific heat capacity (at constant pressure) and density of the nanofluid, respectively. St is Stanton number which is defined according to Eq. (2). Moreover, the first and second terms on the right side of Eq. (1) represent the entropy generation due to heat transfer and fluid friction, respectively.

$$St = \frac{h_{nf} A}{\dot{m} C_{p,nf}} \quad (2)$$

The parameter h_{nf} in Eq. (2) refers to convective heat transfer coefficient of the nanofluid. For a round tube, Eq. (1) could be rewritten as Eq. (3):

$$\dot{S}'_g = \frac{q^2}{\pi k_{nf} T^2 Nu_{nf}} + \frac{32\dot{m}^3 f_{nf}}{\pi^2 \rho_{nf}^2 T D^5} \quad (3)$$

where k_{nf} and Nu_{nf} represent thermal conductivity coefficient of the nanofluid and Nusselt number. By increasing the tube diameter, Re_D decreases; the favorable effect on $\dot{S}'_g$ is that while the heat transfer contribution increases, the fluid friction term decreases.

In order to develop a dimensionless formula for entropy generation rate, the entropy generation number N_s is defined as:

$$N_s = \frac{\dot{S}'_g}{k_{nf} Q^2} \quad (4)$$

By combining Eqs. (3) and (4), the entropy generation number could also be rewritten as:

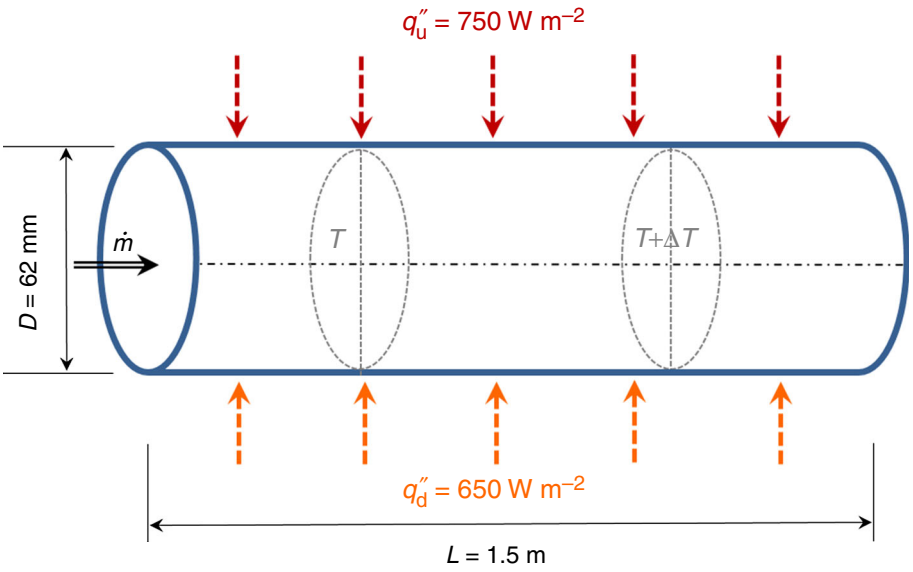

Fig. 1 Schematic diagram of the investigated system

$$N_s = \frac{1}{\pi Nu_{nf}} + \frac{\pi^3 f_{nf} Re^5}{32B^2} \quad (5)$$

where Q, Re and B are dimensionless parameters and defined as Eqs. (6) to (8), respectively.

$$Q = \frac{q}{k_{nf} T} \quad (6)$$

$$Re = \frac{4\dot{m}}{\pi \mu_{nf} D} \quad (7)$$

$$B^2 = \frac{q^2 \rho_{nf}^2 \dot{m}^2}{k_{nf} T \mu_{nf}^5} \quad (8)$$

where μ_{nf} is dynamic viscosity of the nanofluid. As it was mentioned, use of the nanofluid improves heat transfer performance and this improvement depends on its thermophysical properties. Accordingly, the aim of this work is to find the optimum condition of the nanofluid volume fraction (ϕ), nanoparticle diameter (d_p) and Reynolds number (Re).

The dimensionless parameter Bejan number (Be) represents the share of the thermal entropy generation in the total irreversibility (ratio of entropy generation due to heat transfer to the total entropy generation) and defined as Eq. (9) [31, 32].

$$Be = \frac{S_{g,h}}{S_{g,tot}} \quad (9)$$

Thermophysical properties of nanofluids

Determining the thermophysical properties of the nanofluid is an important step in the modeling. In present study, two different metallic oxides (aluminum oxide Al_2O_3 and copper oxide CuO) and one nonmetallic oxide (silicon dioxide SiO_2) are investigated as nanoparticles which are dispersed in 60:40 EG/W (60% ethylene glycol and 40% water by mass) mixture as the base fluid. The details of nanoparticles' specifications which are used in the present research are summarized in Table 1.

Viscosity

There are various correlations for calculating nanofluid viscosity, and each of them is used for specific nanofluid. Vajjha [33] investigated a wide range of data from previous researches and supplemented them with additional measurements to develop a comprehensive equation for calculating nanofluids' viscosity. The correlation developed is valid for all three mentioned nanofluids as below:

$$\frac{\mu_{nf}}{\mu_{bf}} = A_1 e^{(A_2 \phi)} \quad (10)$$

where A_1 and A_2 are constants that depend on size and concentration of the nanoparticles which are listed in Table 2. It should be noted that the above correlation is valid in the temperature range of $273\,K < T < 363\,K$.

The parameter μ_{bf} in Eq. (10) represents the viscosity of the base fluid (60:40% ethylene glycol/water) and is obtained from ASHRAE Handbook [34].

$$\mu_{bf} = A_3 e^{\left(\frac{A_4}{T}\right)} \quad (11)$$

where A_3 and A_4 are constants and have values of $A_3 = 0.555 \times 10^{-3}$ and $A_4 = 2664$ for 60:40% EG/W mixture [34].

Density and specific heat capacity

The density (ρ_{nf}) and specific heat capacity ($C_{p,nf}$) of the nanofluids are obtained by Eqs. (12) and (13), respectively [35, 36].

$$\rho_{nf} = \phi \rho_p + (1 - \phi) \rho_{bf} \quad (12)$$

$$C_{p,nf} = \frac{\phi \rho_p C_{p,p} + (1 - \phi) \rho_{bf} C_{p,bf}}{\rho_{nf}} \quad (13)$$

where ρ_{bf} and $C_{p,bf}$ are density and specific heat capacity of the base fluid and are given by Eqs. (14) and (15), respectively (for 60:40% EG/W base fluid) [34].

$$\rho_{bf} = -0.0024T^2 + 0.963T + 1009.8 \quad (14)$$

$$C_{p,bf} = 4.2483T + 1882.4 \quad (15)$$

Thermal conductivity

Thermal conductivities of aluminum oxide (Al_2O_3) and copper oxide (CuO) nanoparticles with several concentrations in the 60:40% EG/W base fluid were measured by Vajjha and Das [37], and their study was extended to silicon dioxide (SiO_2) by Shahoo [38]. In addition, according to Koo and Kleinstreuer [39], k_{nf} is composed of two terms: the first term is called particle's conventional static part (k_s) and the second one is Brownian motion part (k_B).

Table 1 Properties of investigated nanoparticles in the present study [40]

Nanoparticle/d_p	ρ_p/kg m^{-3}	$C_{p,p}$/J kg^{-1} K^{-1}	k_p/W m^{-1} K^{-1}
Al_2O_3 (45 nm)	3600	765	36
CuO (29 nm)	6500	533	17.65
SiO_2 (20, 50, 100 nm)	2220	745	1.4

Table 2 Constants of Eq. (10) [33]

Nanoparticle	ϕ: concentration	A_1	A_2
Al_2O_3 (45 nm)	$0<\phi<0.1$[a]	0.983	12.959
CuO (29 nm)	$0<\phi<0.06$	0.9197	22.8539
SiO_2 (20 nm)	$0<\phi<0.1$	1.092	5.954
SiO_2 (50 nm)	$0<\phi<0.06$	0.9693	7.074
SiO_2 (100 nm)	$0<\phi<0.06$	1.005	4.669

[a] $\phi = 0.1$ means 10% particle volumetric concentration

$$k_{nf} = k_s + k_B = \frac{k_p + 2k_{bf} - 2(k_{bf} - k_p)\phi}{k_p + 2k_{bf} + (k_{bf} - k_p)\phi} k_{bf} + 5 \times 10^4 \beta \phi \rho_{bf} C_{p,bf} \sqrt{\frac{\kappa T}{\rho_p d_p}} f(T, \phi) \quad (16)$$

In this equation, k_{bf} represents thermal conductivity of the base fluid which is a function of the temperature, obtained from ASHRAE Handbook [34] according to Eq. (17) for 60:40% EG/W mixture. The parameter β represents fraction of the liquid volume which travels with a particle and is a function of particle volume concentration which is obtained from Table 3; also $f(T, \phi)$ is a function of the particle volume concentration and temperature and is calculated by Eq. (20).

$$k_{bf} = -3 \times 10^{-6} T^2 + 0.0025T - 0.1057 \quad (17)$$

$$f(T, \phi) = \left(2.8217 \times 10^{-2}\phi + 3.917 \times 10^{-3}\right)\left(\frac{T}{T_0}\right) + \left(-3.0669 \times 10^{-2}\phi - 3.91123 \times 10^{-3}\right) \quad (18)$$

All of the base fluid properties correlations (Eqs. 11, 14, 16 and 17) are valid within the $293\,K \le T \le 363\,K$ temperature range. The presented results in current study are based on $T = 310\,K$.

Nusselt number and friction factor

Vajjha et al. [40] developed an accurate correlation for calculating Nu number of the Al_2O_3, CuO and SiO_2 nanofluid flow (with 60:40% EG/W base fluid) inside

Table 3 Correlations of the β [37, 38]

Nanoparticle	ϕ: concentration	T: temperature/K	β
Al_2O_3 (45 nm)	$0.01<\phi<0.1$	$298<T<363$	$8.4407(100\phi)^{-1.07304}$
CuO (29 nm)	$0.01<\phi<0.06$	$298<T<363$	$9.881(100\phi)^{-0.9446}$
SiO_2 (20, 50, 100 nm)	$0.01<\phi<0.06$	$298<T<363$	$1.9526(100\phi)^{-1.4594}$

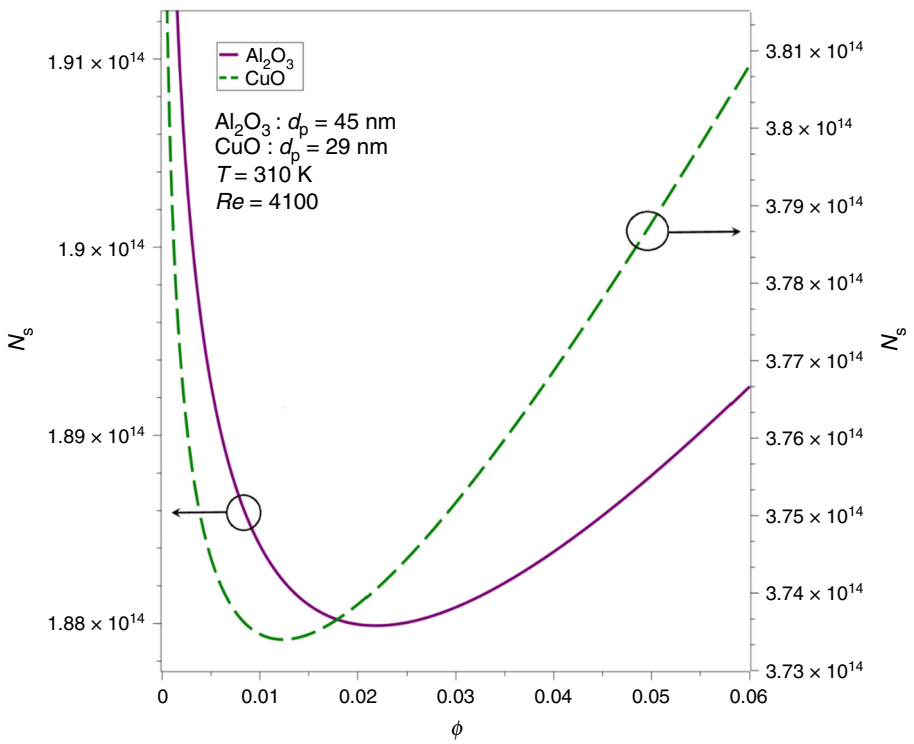

Fig. 2 Variation of entropy generation number as a function of particle volumetric concentration (Al_2O_3 and CuO)

Table 4 Optimal volume fraction for different nanofluids based on using quadratic optimization algorithm

Nanofluid	Admissible volume fraction range	Optimal volume fraction (ϕ_{opt})
Al_2O_3 (45 nm)	$0 < \phi < 0.1$	0.021845
CuO (29 nm)	$0 < \phi < 0.06$	0.012352
SiO_2 (20 nm)	$0 < \phi < 0.1$	0.053787
SiO_2 (50 nm)	$0 < \phi < 0.06$	0.036843
SiO_2 (100 nm)	$0 < \phi < 0.06$	0.027379

circular tube. In Eq. (19), in addition to the *Re* and *Pr*, efforts have been also made to investigate the effect of the particle concentration (ϕ). This correlation showed an average deviation of 2% and maximum deviation of ± 10% in comparison to the experimental data. It should be noted that, the correlation is valid in the range of $3000 < Re < 16,000$ for all three nanofluids; in addition, it is valid in the range of $0 < \phi < 0.1$ for Al_2O_3 nanofluid and in the range of $0 < \phi < 0.06$ for CuO and SiO_2 nanofluids.

$$Nu_{nf} = 0.065\left(Re^{0.65} - 60.22\right)\left(1 + 0.0169\phi^{0.15}\right)Pr^{0.542}; R^2 = 0.97 \quad (19)$$

According to Vajjha et al. [40], the correlation of the friction factor could be written as:

$$f_{nf} = 0.3164Re^{-0.25}\left(\frac{\rho_{nf}}{\rho_{bf}}\right)^{0.797}\left(\frac{\mu_{nf}}{\mu_{bf}}\right)^{0.108} \quad (20)$$

The above correlation (Eq. 20) is valid for the range of $4000 < Re < 16,000$ for all three nanofluids and also is valid in the range of $0 < \phi < 0.1$ for Al_2O_3 nanofluid and in the range of $0 < \phi < 0.06$ for CuO and SiO_2 nanofluids.

As it mentioned, due to having an application for this work, the range of the investigated parameters has been selected for parabolic trough solar collectors. Based on the flow conditions for nanofluid flow inside the absorber tube of the solar collectors and also previous investigations [41, 42] in this field, the investigated range of the parameters is selected as: nanoparticle diameter ($20\text{nm} \le d_p \le 100\text{nm}$), average flow temperature ($273\,\text{K} \le T \le 363\,\text{K}$) and Reynolds number ($4000 \le Re \le 16,000$). The mentioned ranges for d_p, T and *Re* are same for all of the investigated nanofluids; but the studied range of the volume fraction for each nanofluid is according to Table 2.

As it mentioned, the main objective of the present investigation is to minimize entropy generation rate for nanofluid flow inside a tube. Optimization target function is defined as Eq. (3) and then was rewritten in dimensionless form as Eq. (5). Equations (1) to (20) perform the governing equations of the problem which the analytical optimization process is done for them.

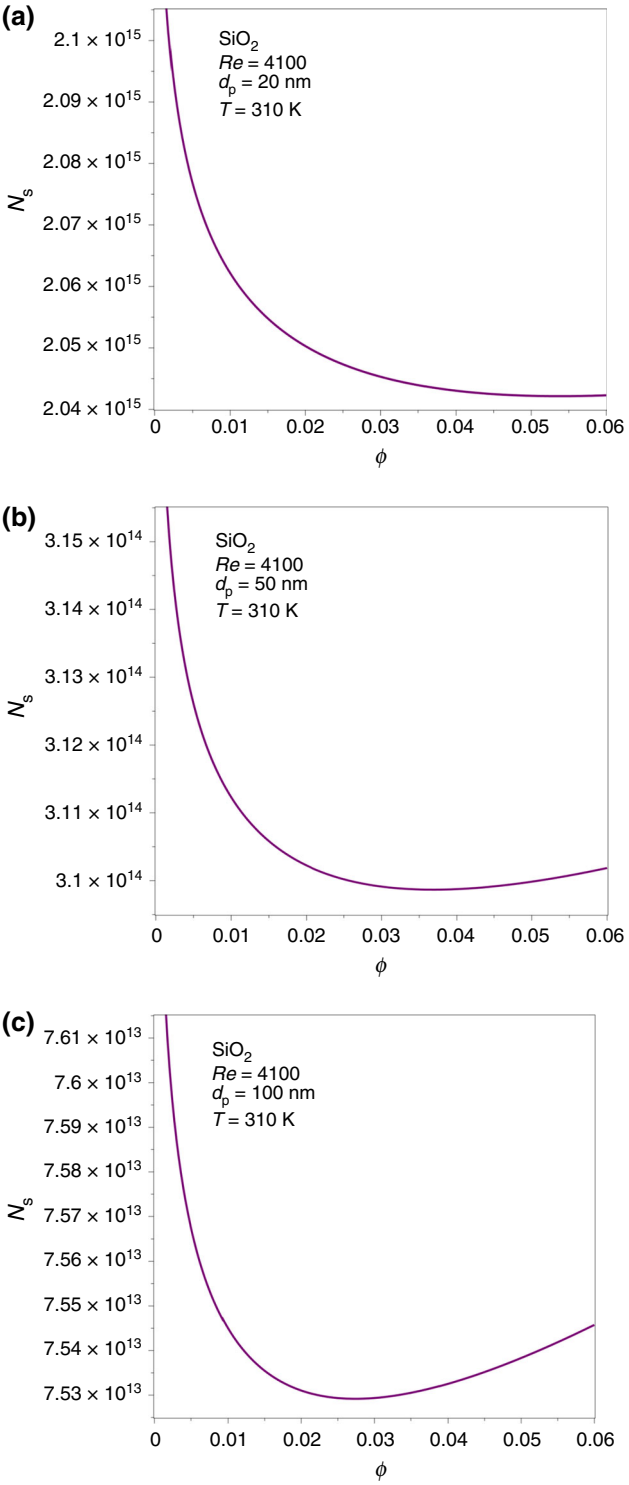

Fig. 3 Variation of entropy generation number as a function of particle volumetric concentration (SiO_2)

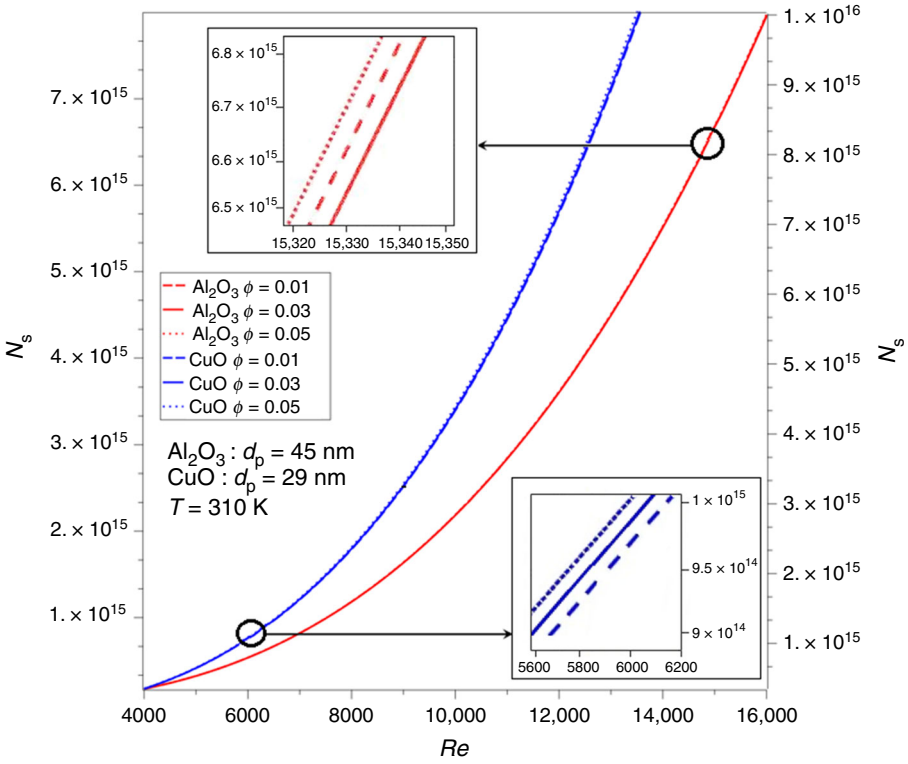

Fig. 4 Variation of entropy generation number as a function of *Re* number (for different volume fractions: Al_2O_3 and CuO)

Results and discussion

A comparison of the entropy generation number in terms of the volume fraction is presented in Fig. 2, for Al_2O_3 and CuO. As shown in this figure, by increasing ϕ to a certain value, N_s decreases; after that, by increasing ϕ the amount of the N_s increases. In the other words, there is an optimal volume fraction (ϕ_{opt}) for all nanofluids in which the entropy generation is minimized. According to the quadratic optimization method and based on the admissible volume fraction of these nanofluids, the optimal volume fraction (ϕ_{opt}) is given in Table 4 for Re = 4100.

Figure 3 shows variation of N_s in term of ϕ for different cases of SiO_2 nanoparticles. According to Fig. 3, by increasing d_p from 20 to 50 nm, the minimum amount of the N_s declined from 2.042×10^{15} to 3.098×10^{14} and this represents a 84.8% reduction in dimensionless entropy generation; this value is 75.7% when d_p rises from 50 to 100 nm.

The two metallic oxide particles (i.e., Al_2O_3 and CuO) have higher values of the influential thermophysical properties (higher density, thermal conductivity, etc.) compared to the SiO_2 nonmetallic oxide nanoparticle. By analyzing the results, it can be concluded that metallic oxide nanoparticles have higher heat transfer coefficient and consequently lower N_s, in comparison to SiO_2. Moreover, between two metallic oxide nanoparticles, CuO is better in comparison with Al_2O_3 due to generating lower entropy.

Figure 4 shows the effect of the Reynolds number variation on the entropy generation for various volume fractions of two metallic oxide nanofluids. It has been obviously proofed that in a thermodynamic system, as the rate of N_s reduces, the system will be optimized better. For instance, according to this figure, for CuO (29 nm) nanoparticle, the lowest amount of the N_s occurs for $\phi = 0.01$; also based on the results of Table 4, by applying quadratic optimization algorithm, the optimal volume fraction is $\phi_{opt} = 0.012352$. Accordingly, it can be concluded that using nanofluid with a volume fraction around its optimal value leads to reduction in the N_s and an optimized thermal system. By increasing volume fraction and *Re* number, it is observed that the nanofluid thermal conductivity increases extremely; consequently, it improves heat transfer and reduces entropy generation as shown in Fig. 4.

Variation of entropy generation number for SiO_2 nonmetallic oxide nanofluid as a function of Reynolds number is plotted in Fig. 5a–c, for various volume fractions. Based on Fig. 5, it can be concluded that increasing the nanoparticle size from 20 to 100 nm results in 85% decrease in maximum amount of entropy generation number. Consequently, it can be concluded that for a constant ϕ, as the size of particles increase, the entropy generation number becomes lower which means that it is better to use the larger particles according to the available diameters.

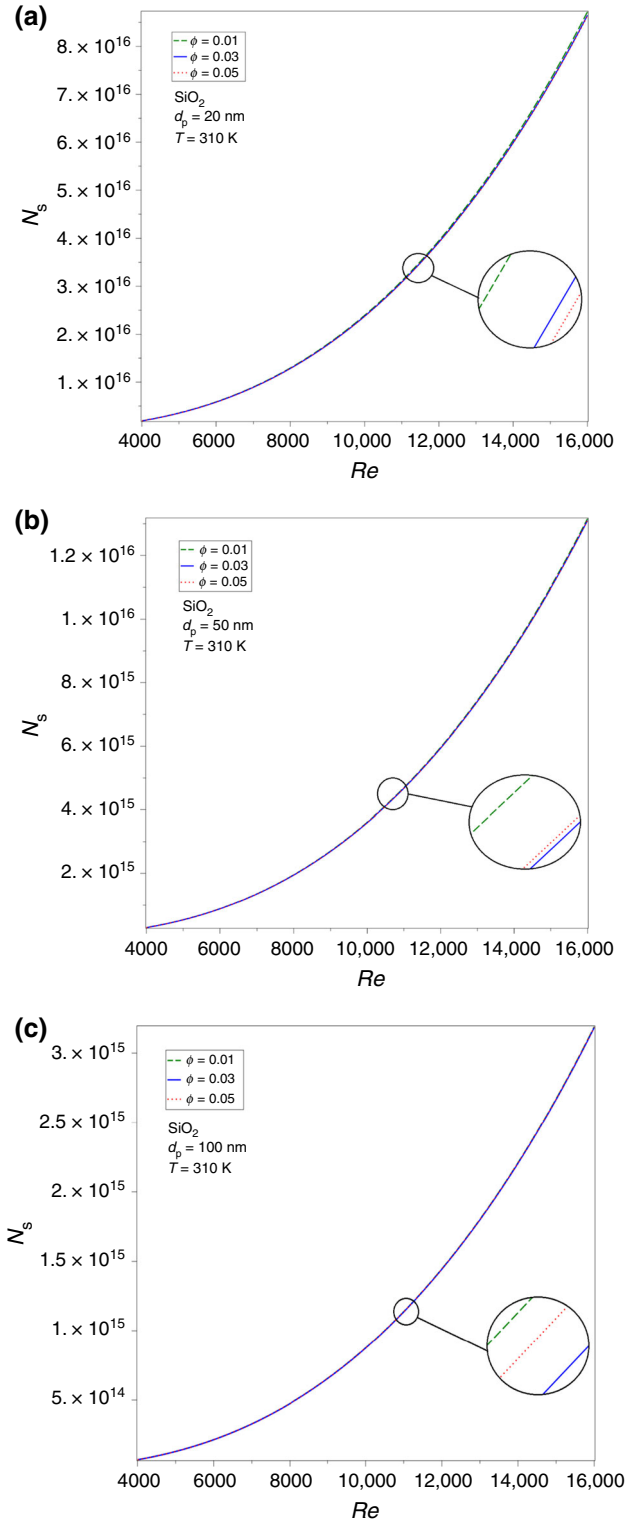

Fig. 5 Variation of entropy generation number as a function of *Re* number (for different volume fractions: SiO_2)

As it can be seen in Figs. 4 and 5, the effect of the nanoparticle concentration on entropy generation rate is low but despite that the optimization process was applied to

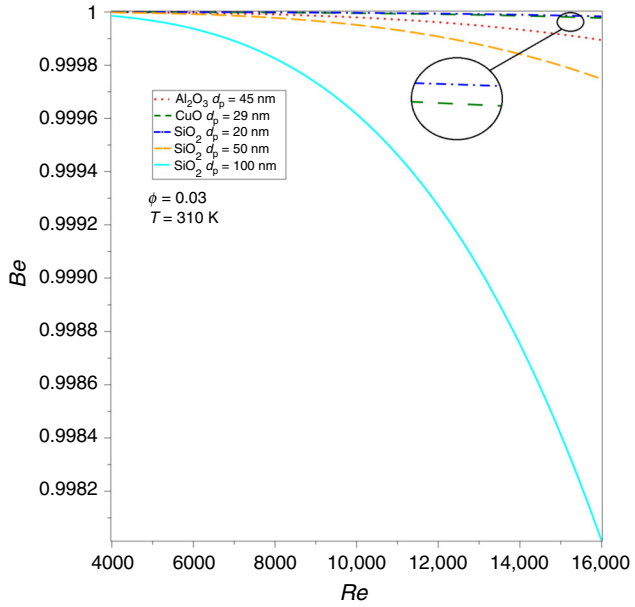

Fig. 6 Variation of Bejan number as a function of Reynolds number

all of the parameters and their optimal conditions was determined.

Figure 6 shows variation of the Bejan number in terms of the Reynolds number for the base fluid and the nanofluids. As it is expected, frictional entropy generation increases with Re number; and thermal entropy generation decreases by increasing Re number. Based on Eq. 11 and the above-mentioned contents, as it can be seen in Fig. 6, the *Be* number decreases by increasing Re number.

Irreversibility distribution ratio is defined as the ratio of frictional entropy generation to the thermal entropy generation ($\Phi = \frac{S_{g,f}}{S_{g,h}}$).Variation of Φ is plotted in Fig. 7. This figure shows that for all the investigated nanofluids, the slopes are ascending (Φ increase with *Re*). By comparing the curve of the two metallic oxide nanofluids (Al_2O_3 and CuO), it is observed that the irreversibility ratio of copper oxide nanofluid is lower than that aluminum oxide nanofluid. Moreover, by comparing SiO_2 curves, it is concluded that by increasing nanoparticle sizes, the irreversibility ratio increases; since *Re* increases, $S_{g,f}$ increases and $S_{g,h}$ decreases.

A comparison of the entropy generation number of the all three nanofluids under investigation is presented in Fig. 8 (for $d_p = 45$nm, $\phi = 0.02$ and T = 310 K). Figure 9 illustrates N_s for various particle sizes ($\phi = 0.02$). As it can be seen in Fig. 8, for the same conditions, SiO_2 has the highest N_s which is due to the fact that it is nonmetallic oxide nanoparticle and two others are metallic oxide. Also by comparing Al_2O_3 and CuO curves in Fig. 8, it is observed that if CuO is used instead of Al_2O_3, the maximum N_s is reduced by 20% (the maximum N_s of CuO in

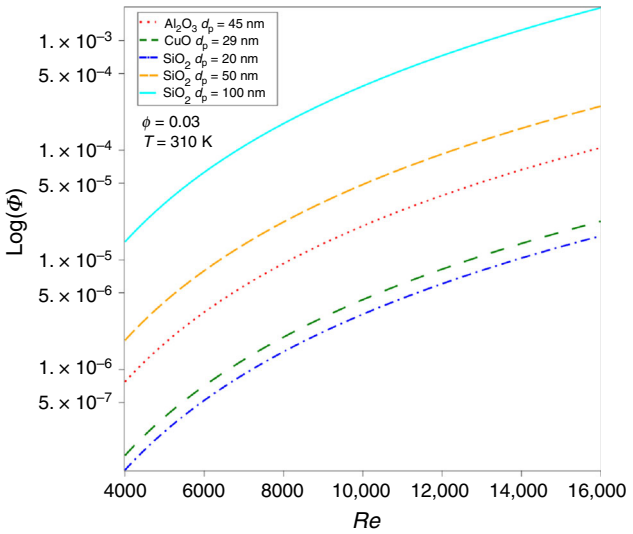

Fig. 7 Variation of irreversibility distribution ratio number as a function of Reynolds number

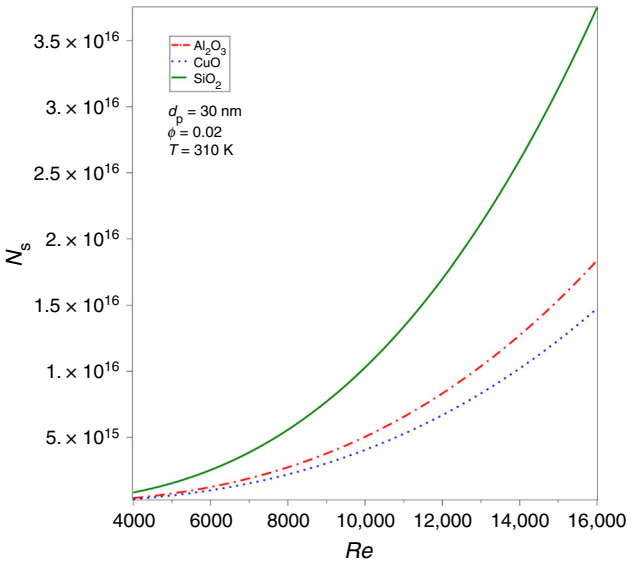

Fig. 8 Comparison of the entropy generation number of nanofluids for the same conditions

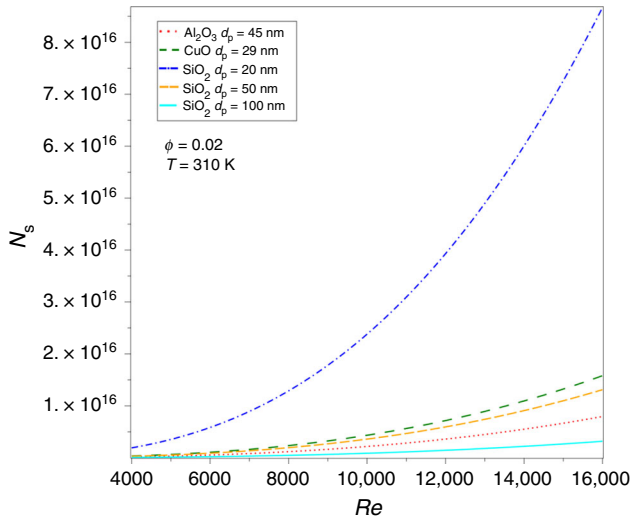

Fig. 9 Comparison of the entropy generation number of nanofluids for the different conditions

Table 5 General optimization value

Nanoparticle	$N_{s,opt}$	ϕ_{opt}
Al_2O_3	$1.2 \times 10^{+12}$	0.033139
CuO	$9.5 \times 10^{+11}$	0.015884
SiO_2	$2.5 \times 10^{+12}$	0.057634

Fig. 9 is 20% lower than Al_2O_3). It means that if all of the effective parameters are considered the same, the use of CuO will make the system more efficient.

As it was mentioned in previous sections, N_s decreases by increasing d_p. Now, by comparing Figs. 8 and 9, it could be seen that by increasing particle size of Al_2O_3 (from 30 to 45 nm) and decreasing particle size of CuO (from 30 to 29 nm), the N_s of Al_2O_2 gets lower than CuO. This represents that excessive increase of nanoparticle diameter will overcome to effect of the other parameters; therefore, by increasing size of SiO_2 nanoparticles to 100 nm, SiO_2 will have the least entropy generation number (even though it is a nonmetallic oxide nanoparticle).

By applying optimization process for $273 < T < 363$ K, $4000 < Re < 16{,}000$, $20 < d_p < 100$ nm and acceptable range of the volume fraction ϕ for each nanoparticle, it is concluded that the optimal value of average flow temperature, Re number and d_p for all cases is 363 K, 4000 and 100 nm, respectively; in addition, the optimal value of ϕ and N_s for each case is represented in Table 5.

By applying optimization process for $273 < T < 363$ K, $4000 < Re < 16{,}000$, $20 < d_p < 100$ nm and acceptable range of the volume fraction ϕ for each nanoparticle, it is concluded that the optimal value of average flow temperature, *Re* number and d_p for all cases is 363 K, 4000 and 100 nm, respectively; in addition, the optimal value of ϕ and N_s for each case is represented in Table 5.

Conclusions

In current investigation, the efforts have been made to optimize the nanofluid turbulent flow inside a circular tube based on the second law of thermodynamics and entropy generation minimization approach. The EGM approach has been used to optimize three effective parameters (ϕ, d_p and *Re*) for three common nanoparticles (Al_2O_3, CuO and

SiO_2) dispersed in a 60:40% ethylene glycol/water as a base fluid. The main conclusions of the present study can be summarized as follows:

- By increasing ϕ to a certain value, N_s decreases; and after that, by increasing ϕ the amount of the Ns increases. Consequently, there is a certain amount of the volume fraction with minimum entropy generation rate which could be considered as the optimal value. The optimal values for Al_2O_3, CuO and SiO_2 nanofluids are 0.033139, 0.015884 and 0.057634, respectively.
- As the particle size increases, the total entropy generation decreases; therefore, by applying larger nanoparticles, a better optimal thermodynamics system could be achieved. For example, with an increase in diameter from 50 to 100 nm, the entropy generation number for SiO_2 reduced by 75%. It should be noted that the size of the nanoparticles must be selected within the permitted range, because in the case of excessive large nanoparticles, the effects of other parameters become negligible.
- In the investigated range of average flow temperature and Re number, the optimum amount is upper value of the range (for average flow temperature) and lower value of the range (for Re number), respectively. In the other words, by increasing average flow temperature and decreasing Re, the amount of total entropy generation is reduced. For example, with an increase in temperature from 310 to 363 K degrees at d_p = 100 nm, it will see a 96% reduction in entropy generation number for SiO_2.
- By applying optimizing process for whole parameters' range and analyzing all of the results, it was found that for the same conditions, SiO_2 has the most and CuO has the least amount of the entropy generation. For example, taking into account all the optimal conditions, the relative percent difference between entropy generation number of CuO and SiO_2 to entropy generation number of SiO_2 is 62%. This is due to the fact that SiO_2 is nonmetallic oxide nanoparticle and two others are metallic oxides.

References

1. Mwesigye A, Huan Z, Meyer JP. Thermodynamic optimisation of the performance of a parabolic trough receiver using synthetic oil-Al_2O_3 nanofluid. Appl Energy. 2015;156:398–412. https://doi.org/10.1016/j.apenergy.2015.07.035.
2. Okati V, Behzadmehr A, Farsad S. Analysis of a solar desalinator (humidification–dehumidification cycle) including a compound system consisting of a solar humidifier and subsurface condenser using DoE. Desalination. 2016;397:9–21.
3. Jamal-abadi MT, Zamzamian AH. Optimization of thermal conductivity of Al_2O_3 nanofluid by using ANN and GRG methods. Int J Nanosci Nanotechnol. 2013;9:177–84.
4. Minea AA, Lorenzini G. A numerical study on ZnO based nanofluids behavior on natural convection. Int J Heat Mass Transf. 2017;114:286–96. https://doi.org/10.1016/j.ijheatmasstransfer.2017.06.069.
5. Minea AA. Comparative study of turbulent heat transfer of nanofluids: effect of thermophysical properties on figure-of-merit ratio. J Therm Anal Calorim. 2016;124:407–16.
6. Ahmadi MH, Ahmadi MA, Nazari MA, Mahian O, Ghasempour R. A proposed model to predict thermal conductivity ratio of Al_2O_3/EG nanofluid by applying least squares support vector machine (LSSVM) and genetic algorithm as a connectionist approach. J Therm Anal Calorim. 2018;123456789:1–11. https://doi.org/10.1007/s10973-018-7035-z.
7. Maganti LS, Dhar P. Consequences of flow configuration and nanofluid transport on entropy generation in parallel microchannel cooling systems. Int J Heat Mass Transf. 2017;109:555–63. https://doi.org/10.1016/j.ijheatmasstransfer.2017.02.036.
8. Ibáñez G, López A, Pantoja J, Moreira J, Reyes JA. Optimum slip flow based on the minimization of entropy generation in parallel plate microchannels. Energy. 2013;50:143–9. https://doi.org/10.1016/j.energy.2012.11.036.
9. Arabpour A, Karimipour A, Toghraie D, Akbari OA. Investigation into the effects of slip boundary condition on nanofluid flow in a double-layer microchannel. Netherlands: J Therm Anal Calorim. Springer; 2017. p. 1–17.
10. Safi MA, Ghozatloo A, Hamidi AA, Shariaty-Niassar M. Calculation of heat transfer coefficient of MWCNT-TiO2 nanofluid in plate heat exchanger. Iran Nanotechnol Soc 2014;10:153–62. http://www.ijnnonline.net/article_9092_10.html.
11. Hosseinnezhad R, Akbari OA, Hassanzadeh Afrouzi H, Biglarian M, Koveiti A, Toghraie D. Numerical study of turbulent nanofluid heat transfer in a tubular heat exchanger with twin twisted-tape inserts. J Therm Anal Calorim. 2017. https://doi.org/10.1007/s10973-017-6900-5.
12. Esfahani JA, Akbarzadeh M, Rashidi S, Rosen MA, Ellahi R. Influences of wavy wall and nanoparticles on entropy generation over heat exchanger plat. Int J Heat Mass Transf. 2017;109:1162–71. https://doi.org/10.1016/j.ijheatmasstransfer.2017.03.006.
13. Bahiraei M, Berahmand M, Shahsavar A. Irreversibility analysis for flow of a non-Newtonian hybrid nanofluid containing coated CNT/Fe_3O_4 nanoparticles in a minichannel heat exchanger. Appl Therm Eng. 2017;125:1083–93. https://doi.org/10.1016/j.applthermaleng.2017.07.100.
14. Delfani S, Karami M, Akhavan Bahabadi MA. Experimental investigation on performance comparison of nanofluid-based direct absorption and flat plate solar collectors. Int J Nano Dimens. 2015;7:85–96. http://www.ijnd.ir/article_15588_2444.html.
15. Meibodi SS, Kianifar A, Mahian O, Wongwises S. Second law analysis of a nanofluid-based solar collector using experimental data. J Therm Anal Calorim. 2016;126:617–25.
16. Gong X, Wang F, Wang H, Tan J, Lai Q, Han H. Heat transfer enhancement analysis of tube receiver for parabolic trough solar collector with pin fin arrays inserting. Sol Energy. 2017;144:185–202. https://doi.org/10.1016/j.solener.2017.01.020.
17. MohammadZadeh P, Sokhansefat T, Kasaeian AB, Kowsary F, Akbarzadeh A. Hybrid optimization algorithm for thermal analysis in a solar parabolic trough collector based on nanofluid. Energy. 2015;82:857–64. https://doi.org/10.1016/j.energy.2015.01.096.

18. Mahian O, Kianifar A, Sahin AZ, Wongwises S. Entropy generation during Al_2O_3/water nanofluid flow in a solar collector: effects of tube roughness, nanoparticle size, and different thermophysical models. Int J Heat Mass Transf. 2014;78:64–75. https://doi.org/10.1016/j.ijheatmasstransfer.2014.06.051.
19. Liu ZH, Li YY. A new frontier of nanofluid research—application of nanofluids in heat pipes. Int J Heat Mass Transf. 2012;55:6786–97. https://doi.org/10.1016/j.ijheatmasstransfer.2012.06.086.
20. Farzaneh-Gord M, Ameri H, Arabkoohsar A. Tube-in-tube helical heat exchangers performance optimization by entropy generation minimization approach. Appl Therm Eng. 2016;108:1279–87. https://doi.org/10.1016/j.applthermaleng.2016.08.028.
21. Gutiérrez F, Méndez F. Entropy generation minimization for the thermal decomposition of methane gas in hydrogen using genetic algorithms. Energy Convers Manag. 2012;55:1–13.
22. Ellahi R, Hassan M, Zeeshan A, Khan AA. The shape effects of nanoparticles suspended in HFE-7100 over wedge with entropy generation and mixed convection. Appl Nanosci. 2015;6:1–11. https://doi.org/10.1007/s13204-015-0481-z.
23. Siavashi M, Jamali M. Heat transfer and entropy generation analysis of turbulent flow of TiO_2-water nanofluid inside annuli with different radius ratios using two-phase mixture model. Appl Therm Eng. 2016;100:1149–60. https://doi.org/10.1016/j.applthermaleng.2016.02.093.
24. Shalchi-Tabrizi A, Seyf HR. Analysis of entropy generation and convective heat transfer of Al_2O_3 nanofluid flow in a tangential micro heat sink. Int J Heat Mass Transf. 2012;55:4366–75. https://doi.org/10.1016/j.ijheatmasstransfer.2012.04.005.
25. Bianco V, Manca O, Nardini S. Performance analysis of turbulent convection heat transfer of Al_2O_3 water-nanofluid in circular tubes at constant wall temperature. Energy. 2014;77:403–13. https://doi.org/10.1016/j.energy.2014.09.025.
26. Singh PK, Anoop KB, Sundararajan T, Das SK. Entropy generation due to flow and heat transfer in nanofluids. Int J Heat Mass Transf. 2010;53:4757–67. https://doi.org/10.1016/j.ijheatmasstransfer.2010.06.016.
27. Torabi M, Torabi M, Ghiaasiaan SM, Peterson GP. The effect of Al_2O_3-water nanofluid on the heat transfer and entropy generation of laminar forced convection through isotropic porous media. Int J Heat Mass Transf. 2017;111:804–16. https://doi.org/10.1016/j.ijheatmasstransfer.2017.04.041.
28. Mwesigye A, Huan Z. Thermodynamic analysis and optimization of fully developed turbulent forced convection in a circular tube with water-Al_2O_3 nanofluid. Int J Heat Mass Transf. 2015;89:694–706. https://doi.org/10.1016/j.ijheatmasstransfer.2015.05.099.
29. Ghasemi SE, Ranjbar AA. Thermal performance analysis of solar parabolic trough collector using nanofluid as working fluid: a CFD modelling study. J Mol Liq. 2016;222:159–66. https://doi.org/10.1016/j.molliq.2016.06.091.
30. Oullette WR, Bejan A. Conservation of available work (exergy) by using promoters of swirl flow in forced convection heat transfer. Energy. 1980;5:587–96.
31. Paoletti S, Rispoli F, Sciubba E. Calculation of exergetic losses in compact heat exchanger passages. ASME AES. 1989;10:21–9.
32. Pascale S, Gregory JM, Ambaum M, Tailleux R. Climate entropy budget of the HadCM3 atmosphere–ocean general circulation model and of FAMOUS, its low-resolution. Clim Dyn. 2010;10:125–39.
33. Vajjha RS. Measurements of thermophysical properties of nanofluids and computation of heat transfer characteristics. University of Alaska Fairbanks; 2008.
34. Lajos K. International news No uvelles in terna tionales. 1979;56–7.
35. Al-Ansary H, Zeitoun O. Numerical study of conduction and convection heat losses from a half-insulated air-filled annulus of the receiver of a parabolic trough collector. Sol Energy. 2011;85:3036–45. https://doi.org/10.1016/j.solener.2011.09.002.
36. Bellos E, Tzivanidis C, Tsimpoukis D. Thermal enhancement of parabolic trough collector with internally finned absorbers. Sol Energy. 2017;157:514–31. https://doi.org/10.1016/j.solener.2017.08.067.
37. Vajjha RS, Das DK. Experimental determination of thermal conductivity of three nanofluids and development of new correlations. Int J Heat Mass Transf. 2009;52:4675–82. https://doi.org/10.1016/j.ijheatmasstransfer.2009.06.027.
38. Sahoo BC. Measurement of rheological and thermal properties and the freeze-thaw characteristics of nanofluids. University of Alaska Fairbanks; 2008.
39. Koo J, Kleinstreuer C. A new thermal conductivity model for nanofluids. J Nanoparticle Res. 2004;6:577–88.
40. Vajjha RS, Das DK, Kulkarni DP. Development of new correlations for convective heat transfer and friction factor in turbulent regime for nanofluids. Int J Heat Mass Transf. 2010;53:4607–18. https://doi.org/10.1016/j.ijheatmasstransfer.2010.06.032.
41. Mwesigye A, Meyer JP. Optimal thermal and thermodynamic performance of a solar parabolic trough receiver with different nanofluids and at different concentration ratios. Appl Energy. 2017;193:393–413. https://doi.org/10.1016/j.apenergy.2017.02.064.
42. Menbari A, Alemrajabi AA, Rezaei A. Heat transfer analysis and the effect of CuO/Water nanofluid on direct absorption concentrating solar collector. Appl Therm Eng. 2016;104:176–83. https://doi.org/10.1016/j.applthermaleng.2016.05.064.